APPLICATION OF SYNTHETIC APERTURE RADAR (SAR) TO SOUTHERN PAPUA NEW GUINEA FOLD BELT EXPLORATION*

James M. Ellis and Frank D. Pruett
Chevron Overseas Petroleum Inc.
6001 Bollinger Canyon Road
San Ramon, California 94583-0946, U.S.A.

ABSTRACT

Niugini Gulf Oil Pty. Ltd., as operator for two exploration licenses within the southern Papuan Basin fold and thrust belt, has successfully used synthetic aperture radar (SAR) to map surface structure, stratigraphy, and to help in planning a hydrocarbon exploration program.

Rugged karst topography developed on massive Tertiary limestone causes the region to be exceedingly dangerous, if not impossible, to traverse on the ground. The area is seldom cloud free, is covered with tropical rain forest, and geologic field studies are limited. The region is ideally suited to geologic analysis using remote sensing technology. Landsat images and vertical aerial photographs complement SAR but provide subdued structural information because of the jungle cover and minimal shadowing (due to high sun angles). SAR provided our explorationists with an excellent data base because (1) structure is enhanced with low illumination, (2) resolution is 6 x 12 m, (3) digital reprocessing is possible, and (4) clouds are penetrated by the SAR.

Stereoscopic analysis of SAR provided essential geologic information that was used to guide ongoing field work, modeling of subsurface structure, and selecting of well locations. Surface data, including SAR, are used in place of seismic technology as the primary exploration tool in this area because surface conditions limit acquisition of acceptable seismic data at reasonable cost.

SAR imagery revealed significant mass wasting that led to re-evaluation of previously acquired field data. Lithologies were recognized on the radar imagery by textural and tonal changes in spite of the continuous canopy of jungle. The characteristic radar signature of karst topography enabled some limestone-capped, fold and thrust structures to be interpreted beneath thin veneer of volcanics. Reprocessing and contrast stretching of the digital radar imagery allowed additional geologic information to be extracted from the survey in oversaturated (bright) or flared zones.

1.0 INTRODUCTION

Synthetic aperture radar (SAR) imagery was acquired over an area covering Petroleum Prospecting Licenses PPL-17 and PPL-18 during February 1985. These data were acquired in order to help Niugini Gulf Oil Pty. Ltd. and Joint Venture Participants to: (1) map surface geologic structure and stratigraphy, and (2) provide data to assist in planning and conducting the exploration program for hydrocarbons. More than 26,000 km^2 were surveyed with airborne radar (Figure 1). Individual flight strips side-lapped by ~60%, permitting stereoscopic analysis of the terrain. The imagery was

*Presented at the Fifth Thematic Conference: "Remote Sensing for Exploration Geology," Reno, Nevada, September 29-October 2, 1986.

recorded digitally and then plotted at a scale of 1:250,000. A mosaic at the same scale was also constructed.

Interpretation of the radar data was facilitated by previously acquired and ongoing field geology programs within the two permit areas and was complemented by Landsat MSS imagery, aerial photographs, topographic maps, and published geologic maps.

The purpose of this paper is to demonstrate how interpretation of SAR and stereoscopic SAR markedly improved our understanding of surface geology in the southern fold and thrust belt of Papua New Guinea. This paper discusses some of the strengths and weaknesses of other data sets (Landsat, aerial photographs, existing maps, field work) in this isolated, tropical mountainous environment. The limitations of airborne radar imagery (and ways to minimize these limitations) will also be discussed.

The region is largely uninhabited, and is covered by a dense rain forest that approaches 30-40 m (±) in height (Figure 2). Massive Darai Limestone (Tertiary) crops out extensively across the exploration area. The limestone and high rainfall have produced a rugged karst topography that is exceedingly dangerous, if not impossible, to traverse on the ground. The rocks are folded and thrust into large anticlines. Several exceed 25 Km in length (Figure 3). The relief of some of these anticlines approaches 1500 m. The area is seldom cloud free and geologic field studies are limited in extent. Obviously the region is ideally suited for geologic analysis using remote sensing technology.

Sabins (1983) demonstrated the usefulness of space shuttle SAR for interpreting the geology of nearby Indonesia, a country also characterized by persistent cloud cover. Airborne, real-aperture radar (SLAR) was successfully used to compile geologic reconaissance maps for petroleum exploration in cloud-covered Eastern Panama and Northwestern Colombia (Wing and MacDonald, 1973) and in Irian Jaya, Indonesia by Chevron (1972-75).

Exploration evaluation, including drilling, is underway within these licenses in search of liquid hydrocarbon reserves which may be trapped in economic quantities in some of the large structures. Hydrocarbon traps within most exploration provinces are usually defined with seismic technology prior to costly drilling; however, deep karst weathering of surface and near-surface limestones within these licenses limit acquisition of interpretable seismic data at reasonable cost. Typical subsurface information that is required prior to drilling (depth and configuration of reservoir, thickness of stratigraphic units, fault attitudes and throw) is primarily interpreted from imagery, surface observations and sparse well data.

It has been shown that surface-geologic data (dip and strike of bedding, structural plunge, stratigraphic thickness, etc.) can be used to geometrically model subsurface structure in many fold and thrust belts (Dahlstrom, 1969; Hobson, 1986). The better the surface data, the better the subsurface interpretation. We have found stereoscopic SAR to be of significant value in our surface mapping and a tool that has improved subsurface geologic interpretation. In addition, the capacity of modern, airborne SAR imagery to be clearly and accurately enlarged to a working scale of 1:50,000 facilitates: (1) accurate location of field measurements, (2) evaluating potential well locations, (3) checking prior mapping, and (4) planning future field programs to solve critical geologic questions.

2.0 GEOLOGIC DATA AVAILABLE PRIOR TO SAR

2.1 Geologic Maps

Three geologic maps with explanatory notes that cover most of the exploration area have been published at a scale of 1:250,000 by the Australian

Bureau of Mineral Resources and the Papua New Guinea Department of Lands, Surveys and Mines. These maps are the Blucher Range (or OK Tedi), Wabag, and Kutubu sheets (Sheets SB/55-7, -8, and -12, International Index, respectively). The three sheets are compilations of arduous field work and careful photogeology carried out since the 1940's (see Figure 3 for sample). Limited traverses across the rugged anticlines provide dip, strike, stratigraphic contacts, and plunge information. These data, along with more recent field surveys, helped provide constraints on the interpretation from stereoscopic radar strips.

Estimating dip from radar imagery is difficult because no real parallax exists. Vertical exaggeration varies across each radar flight strip due to changing depression angle of the microwave beam (from about 8° to 27° below the horizontal; see Figure 4). Stereoscopic viewing is possible because of small displacements in terrain features and differences in shadow length on adjacent flight strips (R. H. Gelnett and F. F. Sabins, 1986, pers. comm.). A 30° slope on the ground will appear much different to the viewer depending on its position on the radar flight strip. In addition, inherent problems with radar arise because of "layover" (steep slopes leaning into the direction of radar acquisition). Layover causes geometrical inconsistencies (Sabins, 1986). Experience interpreting stereoscopic radar images is required to minimize error in estimating structural dip and plunge.

Geologic mapping indicates surface strata in the area to be predominantly massive Tertiary limestones (the Darai Formation), younger Tertiary siliciclastics, and late Pliocene-Pleistocene volcanics. Typically the anticlines have been formed as the structurally competent Darai Limestone was moved southward, above decollemont surfaces, and thrust over itself or the younger Orabadi (predominantly shale) Formation. This limestone is relatively more resistant to erosion and forms the surface outcrop and topographic relief over most of the anticlinal structures in the licenses. The major structural trend and topographic grain is northwest-southeast.

Volcanic cones began to form during late Pliocene time. Most are steep-sided, conical, strato-volcanoes with deeply dissected slopes and central craters; they are thought to be dormant or extinct (Brown and Robinson, 1982). Published geologic maps indicate a considerable portion of the study area is covered with volcanic rocks. Structural information associated with the folded and thrusted Tertiary rocks is largely lacking where volcanic debris has been mapped. However, as will be shown, the SAR data provide information in some areas which enabled some of the buried stratigraphy and structure to be interpreted beneath the volcanics.

2.2 Topographic Sheets

Excellent topographic sheets were generated from stereoscopic aerial photographs by the Royal Australian Survey Corps (scale 1:100,000; 40 m contour interval). Inherent distortions in the radar imagery due to layover in the high relief areas were minimized by transferring the SAR interpretation onto these topographic sheets. Subtle topographic contour inflections, trends, and slopes frequently have geologic significance which can be observed employing stereoscopic analysis of the SAR flight strips (see Figure 3). Changes in slope and elevation due to lithology or structure; linear trends revealed by fractures, karst trends, streams, and ridges; and oversteepened curvilinear features such as landslide scarps that were seen on the radar image could easily be located within the contour pattern of the 1:100,000 topographic sheets.

2.3 Landsat Imagery

Landsat MSS imagery is available with <20% cloud cover over the southern foldbelt of Papua New Guinea. Chevron Oil Field Research Company digitally processed two scenes to enhance color contrast and emphasize linear features.

As of this date, no TM imagery has been acquired over the southwestern Pacific because no data relay satellite (TDRS) is available for the region.

Standard color IR composites (BGR = 457) of the MSS data are almost completely red because of the extensive forest cover. Nevertheless, there is more information in the interactively processed, color IR images than in standard product images. Agricultural patterns and plots of land that have been slashed and burned dominate the lower flanks of the volcanoes north of the exploration licenses. Recent landslides on the limestone-capped anticlines are clearly revealed as white patches in an otherwise red landform. Vegetation changes with altitude across major anticlines can be detected, and in the lowlands tonal variations that may relate to drainage/topography anomalies and subsurface structure have been observed.

However, Landsat (and vertical aerial photographs) have subdued structural information because of the near-continuous jungle cover and minimal shadowing (the sun is 45 to 50° above the horizon on our Landsat MSS images at 9:30 AM local time).

2.4 Literature

Well illustrated publications for the southern fold belt of Papua New Guinea include the previously mentioned geologic maps with explanatory notes (Davies and Norvick, 1974; Davies, 1983; Brown and Robinson, 1982), Dow's (1977) geological synthesis, and Jenkins' (1974) structural analysis.

Radar technology and geologic interpretation of radar imagery are explained by Sabins (1983, 1986), Wing and MacDonald (1973), and Jensen and others (1977). The latter reference pertains to synthetic aperture radar data that are recorded as a hologram on film. For this survey the SAR data were recorded digitally.

3.0 SAR SURVEY DESIGN

Topography rises steeply toward the north, structure trends northwest-southeast, and thrusting is predominantly directed toward the southwest. Flights paths were east-west with the microwave beam directed northward to minimize shadowing and enhance detection of south-facing bedding and thrust fault traces. Also, by directing the beam at an acute angle to the structural grain, excessive signal returns (signature flare), caused by the many slopes and cliffs that face southwest, were reduced.

Although this survey design provided for the most economical and complete data acquisition, viewing the imagery with north up (shadows directed toward the top margin of the image) typically results in topographic inversion. Most of the radar imagery in this paper is arranged conventionally with north up. The reader may need to rotate this imagery 180° so that north and the shadows are projected downward in order to see the topography in proper perspective (ridges as highs and valleys as lows).

The airplane flew at an altitude of 9 km (30,000 ft) above ground level. Recording of the microwave returns was time-delayed an average of 18 km ground distance, resulting in a near range depression angle of 27° (Figure 4). Data were recorded from 18 km to 63 km for an image swath of 45 km. The depression angle of the radar beam in the far range was 8°. The stereoscopic overlap allowed shadowing to be relatively consistent near joint lines on the mosaic; it was constructed with an average depression angle of 17° (R. H. Gelnett, 1985, pers. comm). A non-stereo survey would have resulted in a poorer mosaic with "joint lines" between flight strips having long shadows of the far range juxtaposed next to short shadows of the near range.

The angle of incidence that the microwaves made with the terrain was

low, accentuating (through shadowing) subtle topographic relief, fracture patterns, and shallow-dipping beds. The drawback of such a low beam was an increase in the amount of area concealed in shadow in regions of high relief. This detrimental shadowing was minimized by analyzing the near range portion of the flight strips (Figure 5). Digital reprocessing of near-range radar imagery cannot improve those areas that are in shadow because there are no data in shadowed areas.

4.0 COMPARISON OF RADAR WITH COLOR PHOTOGRAPHS

Photographs taken during a helicopter field trip in November 1985 allow a comparison between oblique color photographs and corresponding radar images (Figure 6). Visible light and the microwave radar beam (0.4-0.7 μm and 3 cm long wavelengths, respectively) are both reflected from the near-continuous jungle canopy. Radar does not penetrate vegetation because the structure and water of leaves and limbs reflect the microwave energy (see Sabins, 1986).

Figure 6 shows a color photo contrasted with a close-up of radar imagery that covers the same geographical location; however, scale and viewing angle are different. The color photo demonstrates that the jungle canopy conforms with the relief of the underlying terrain; however, the top of the canopy is smoother than the ground surface. The radar-imaging process "smooths" the terrain even more because it averages the returned energy into synthetic 6 x 12 m ground-size cells. These cells have the effect of a low-pass filter. They minimize high frequency relief/reflectance signals. The resultant enhancement of longer wavelength features appears to reveal fundamental geologic features better than the color photos.

5.0 MINIMIZING RADAR SHADOW

The radar mosaic, which utilized the mid-range portion of each flight strip (17° depression angle), has shadows on the north side of major topographic highs that obscure terrain. However, in the near-range portion of the strips much more terrain is illuminated by the steeper depression angle (Figure 5). Within areas on adjacent flight strips that have unequal shadowing (such as the stereopair of Figure 7), it was found that during stereoscopic viewing the "illusion" of topographic relief was maintained in areas where one strip had the terrain illuminated (near-range portion) and the other strip had total shadow (mid- to far-range portion). This sense of topographic relief in areas that were illuminated on only one strip greatly enhanced the interpretation. The foregoing is important for exploration purposes because topography in such a young fold and thrust belt largely reflects geological structure (topographic highs often relate to surface structural culminations or anticlines; topographic lows tend to be zones of weaknesses, faulting, or synclines).

In the near range of individual flight strips, the side of a topographic high that faces away from the radar beam and the area that is cast in shadow cannot provide any information to the interpreter. Flying an entire survey with two look directions (opposite or orthogonal) can nearly eliminate this problem. However, a single, reverse-look flight strip across terrain heavily shadowed in the regional survey would markedly improve the data content across an area 45 km wide. A recent SAR survey planned jointly by Chevron and the contractors utilized a single, reverse-look swath to markedly reduce lost information due to shadowing at a nominal cost.

A Landsat image and a corresponding radar flight strip can be viewed as a stereopair to integrate their different data content, provided both data sets are at the same scale (Figure 7). However, because this exploration area is south of the equator, shadows can be cast toward the west-southwest on Landsat. These shadows oppose the northward-directed radar shadows and create eye strain during stereoscopic viewing.

6.0 STRUCTURAL ANALYSIS WITH SAR

In the subject area the radar image, especially when viewed stereoscopically, is superior to Landsat and aerial photographs for interpreting geologic structure. SAR clearly reveals more geologic information than shown on the published geologic maps (Figures 7-9). With SAR, strikes and dips, anticlines and synclines, and structural plunge can be mapped across terrain where little or no field work has been done.

SAR imagery was used successfully to identify major structural zones throughout the area using standard photogeologic mapping techniques and the stereoscopic radar flight strips. In one area, stratigraphic and structural continuity was interpreted for over 100 km along strike. These interpretations greatly simplify the modeling of subsurface structure associated with hydrocarbon entrapment.

The Amdi, Emuk, and Kaban Ranges are obscured in cloud cover on Landsat and lack detail on the published geologic map (Figure 7). However, the SAR imagery reveals a major fracture pattern that cuts across structure, provides a sense of displacement on many faults, and shows at least two anticlines not mapped on the published geologic sheets. We outlined these previously unmapped structures on the topographic sheets of the area to generate a detailed, surface-structure map using SAR stereoscopic imagery.

Volcanic cones imaged with SAR expand our knowledge of volcanic activity. The degree of dissection (moderate in Figure 8) gives a clue as to the time that volcanic activity ceased. The relationship of the volcanic strata with underlying structure gives a sense of timing for the development of anticlines and synclines in the area; this may be determined from the stereoscopic SAR. The volcanic strata may be (1) in stratigraphic continuity (folded) with the folded structures underneath (suggesting volcanism accompanied or predated the folding), (2) undisturbed or draped over pre-existing folds (suggesting the cones post-date the folding), or (3) markedly disrupted by faults and stratigraphic unconformities (suggesting the cones pre-date the folding).

The age of the volcanic cones and the relationship of cones with the underlying folds provide an estimate for the time of possible trap formation within anticlines.

Determining the extent of faulting (vertical and horizontal displacement, overall length) is of interest to our exploration programs. An example of correlating faults on geologic maps with radar imagery is shown in Figure 9. Two arrows on the radar image highlight a band of upturned, resistant strata that form a sharp topographic break. In the southeastern portion of this zone, a thrust fault is mapped on the geologic sheet. This fault is terminated as it trends northwest on the published map.

The radar image reveals the complex nature of this mapped fault and the surrounding terrain. The upturned strata appears to be topographically higher toward the northwest (left arrow on the radar image) where the Darai Limestone dipslope (Tr on Figure 9) grades smoothly into the plunging nose of the Juha anticline. Here there is no sharp topographic break at the Tr/Tma stratigraphic contact (see Figure 9) as there is farther east where the fault is mapped at the surface. The radar image can be interpreted with the mapped fault losing throw toward the northwest and becoming a blind thrust fault (not reaching the surface).

Two geologic sheets are joined along a north-south line in Figure 9. The SAR image helps extrapolate the greater detail of the eastern sheet onto the western sheet and enables smooth continuation of geology across the boundary.

7.0 STRUCTURES BENEATH THIN VOLCANIC FLOWS

The widespread Darai Limestone weathers to rugged karst topography that has a characteristic radar signature. The radar image of this limestone has an uneven, pitted appearance that is often dissected by long, linear grooves. Tones on the SAR images range from dark to bright on Darai-capped structures (see Figure 3) because of the irregular topography. Resistant limestone pinnacles over 40 m high, sinkholes with surface openings in excess of 100 m, and deeply weathered fractures dominate the surface of the Darai. Resistant strata within the Darai Limestone crop out with an irregular pattern due to the rugged surface morphology.

Pliocene to Pleistocene volcanics cover large portions of the fold and thrust belt. On the radar imagery, the surface morphology of some of the volcanic deposits can appear as karst terrain with well-developed sinkholes, pinnacles, and linear troughs. Here it is inferred that the Darai Limestone is buried beneath the volcanic cover. The radar is reflected from trees growing on the volcanics, generating a subdued but characteristic radar signature for the Darai Limestone (Figure 10).

The timing of the volcanic deposition and the formation of karst topography is poorly understood. The development of karst in the Darai Limestone may have been before or after the deposition of the volcanic debris (see Figure 10). Radar imagery is not conclusive; field work is required. Speleological expeditions along the northeastern margin of the PPL-17 and -18 exploration licenses indicate karsting was initiated in Late Pliocene to Early Pleistocene time (Francis and others, 1980, p. 111).

In addition, the timing of volcanism with folding and thrusting of the underlying Darai Limestone is not clear. As noted before, the volcanics may unconformably overlie the folds but in some areas are not thick enough to conceal them, or the volcanics may have been deposited as a "flat" blanket that subsequently was deformed by folding and thrusting (Figure 11).

Pliocene to Pleistocene volcanics are mapped (Brown and Robinson, 1982) across most of the area shown in Figure 11 (for regional see Figure 3). Two volcanic units dominate: TQvs (andesitic and basaltic agglomerates, tuff and lava...) and TQsl (volcaniclastic andesitic and basaltic breccia, reworked agglomerate, tuff, ...exotic blocks of limestone...). Agglomerates are chaotic assemblages of coarse, angular pyroclastic material - formed by volcanic explosion or aerial expulsion from a volcanic vent.

The geologic map (Figure 11) shows two faults, trending NW-SE, that converge toward the southeast, near "Landslide Mountain". The Darai Limestone (Tmd) caps an anticline (seen toward the northwest) that is mapped with an anticlinal axis symbol; this symbol terminates at the edge of the volcanics (TQsl). With the accompanying SAR image, this axis can be extrapolated southeast under the volcanics, and the plunge of the anticline can be inferred. Dip and strike information along the trend of this buried anticline also can be determined stereoscopically from SAR.

8.0 MASS WASTING

The high relief, heavy rainfall, pronounced undercutting of steep slopes by surface rivers, and extensive subsurface erosion caused by karst phenomena (solution and sapping) have resulted in widespread mass wasting in the fold and thrust belt. Giant landslide blocks and scarps can be confused with tectonic features or <u>in-situ</u> bedding, which leads to poorer structural interpretations. The radar images enabled us to recognize numerous mass-wasting zones and alerted us to re-evaluate published dips and strikes in the affected areas.

The detection of mass-wasting features on SAR helps on-going field

work by locating areas with fresh outcrops. Detection of faults, fractures, or stratigraphic unconformities within areas of mass wasting is effectively accomplished with stereoscopic SAR, unless the features are hidden by radar shadows. Satellite imagery, aerial photographs, and/or field work must be employed in shadowed areas.

One of the largest anticlines in the subject area (Mananda, Figure 3) has significant mass wasting along its flanks. The topographic slope along the northeastern nose is extreme (see simplified topographic map - 400 m contour interval, Figure 3). Vertical relief changes >1000 m over a horizontal distance of <4000 m. Here the Hegigio River is cutting a steep gorge. Rock slides are readily seen on the Landsat image (Figures 3 and 12). The bright white patch on the Landsat is a recent rockslide that exposes 1 km of fresh Darai Limestone. The limestone strata are steeply dipping and unvegetated. These rock slides are evident but partially hidden in shadow on the radar mosaic, and they are not mapped on the geologic sheet.

On the radar image, large WSW-ENE topographic breaks are recorded that cut the eastern nose of the anticline; these are very subtle on Landsat and unmapped on the geologic map (Figure 12). The downward extent of these breaks is unknown. They may affect reservoir continuity at depth, or they may be restricted to the Darai Limestone cap and represent giant blocks moving downslope toward the down-cutting Hegigio River (see Figure 3). The anticline steps down hundreds of meters toward the southeast across these blocks. The Hegigio River gorge, where it crosses and truncates the nose of the Mananda anticline, may reveal a zone of weakness at depth.

At other anticlines in the area, SAR clearly reveals large slump blocks caused by rivers undercutting and oversteepening the anticlines' flanks. These blocks have an arcuate headward scarp opening toward the downslope valley. Accurate mapping of these actively eroding landforms is a prerequisite for pipeline and logistical planning within the valleys of the area.

A north-south field traverse crossing the southern flank of Mananda is shown on the geologic map by dip and strike symbols (Figure 3). Examination of the radar image reveals an apparent topographic depression along this southern flank that is also marked on the topographic map by an increase in the horizontal distance between the 800 and 1200 m contour lines (Figure 3). Elevations decrease by 1000 m from the anticlinal axis to this synclinal axis, across a horizontal distance of only 6000 m. This steep relief has facilitated massive rock slides and slumps of the Darai Limestone caprock. Fissures and erosional scarps (generally parallel to topographic contour) and lobes of slumped material occur along the entire southern flank of Mananda. Many fractures cut across the axis of this anticline. These fractures can be followed from the stable crest southward where they are often aligned with an edge of a slump or slide scar.

Dips and strikes determined in the field on the southern flank of Mananda must be reconciled with the radar evidence of severe surface disruption (Figure 3). Interpretation of reservoir geometry and depth based on surface evidence may be in error if SAR is not used to detect mass wasting.

Down-dropped blocks of Darai Limestone (to 2 x 2 km in area) along the extended crests of anticlines have been detected with SAR (Figure 13). Such depressions may reflect (1) structurally controlled, downdropped grabens due to crestal extension during folding, (2) zones of thinner limestone created by increased subsurface erosion (water, solution, and sapping concentrated by associated fracture systems), (3) incipient rock slides caused by fluvial erosion at the base of the anticline's flanks, or (4) the surface expression of a deep fault and fracture system that has major exploration significance. Only field work and drilling can determine what geological process(es) controls the development of crestal depressions.

9.0 LITHOLOGIC DISCRIMINATION

Although the terrain is covered with a jungle canopy, many lithologies can be recognized by their characteristic radar signatures (see Sabins, 1983). The typical slope, relief, and resistivity to weathering of each lithologic category affects the morphology of the terrain. This typical morphology is reflected in the surface of the jungle canopy and is imaged with SAR.

The Darai Limestone, a resistant ridge former that is prone to intense karst weathering, is easily identified (see Figure 3). Non-resistant slope formers (Tertiary mudstones, shales and siltstones) are shown in Figure 6. Quaternary alluvium, a medium-gray, flat surface on SAR, is also easily identified in the bottoms of valleys (Qk on Figure 11).

However, localized field work associated with our exploration program differentiated the Tertiary sedimentary rocks into (1) stratified volcaniclastics, (2) siltstones, (3) a weak limestone unit, and (4) the more resistant Darai Limestone (Figure 14). These four units crop out along relatively flat to gently sloping terrain (Figure 14). The accompanying radar image has labeled arrows pointing to areas where the field work confirms the type of rock cropping out beneath the jungle canopy.

The stratified volcaniclastics (generally Tpw on the geologic map, Figure 14) are seen on the SAR and in the field as beds with characteristic resistant strata. This rock type crops out along the southern margin of the Juha anticline and also along the northern flank in a northwest-southeast trending band. On the geologic map, Tpw is only mapped along the southern perimeter of the anticline.

Darai Limestone has a more limited outcrop pattern on the radar imagery as compared with the map (Figure 14). The radar shows it cropping out within a gorge that cuts across the anticline, but there does not appear to be the typical radar signature of the Darai along the crest of the anticline as depicted on the map. Along the crest the radar records a grainy, coarse texture that is seen in the field as a siltstone. A weaker limestone (generally Tma on the map) is imaged by SAR with a lighter tone and slightly smoother texture than the siltstone. These subtle radar and field observations about lithology can be extrapolated to areas where no field data exist to improve surface stratigraphic maps and, therefore, subsurface structural interpretations.

The radar image in Figure 14 is from a mosaic composed of 1:50,000 enlargements of the near- and mid-range portions of two flight strips. The splice lines can be seen intersecting near the center of the SAR image in Figure 14. It can be seen that radar signatures for the same lithology vary across the east-west splice line. The northern and the southern strips have ~8° and ~17° depression angles along the east-west splice line, respectively. Differences in the intensity of radar returns and; therefore, the resulting image signatures (Sabins, 1983) may result from the different depression angles.

10.0 DIGITAL REPROCESSING OF SAR IMAGERY

Reprocessing of the digital data allowed additional geologic information to be extracted from the survey. The original photographic strips were contrast-balanced for the entire scene. However, cliffs that faced the radar antenna reflected (as expected) a relatively high amount of radar energy, which resulted in oversaturated (bright) or "flared" zones on the original strips (Figure 15A).

The radar digital data shown in Figure 15A and B were resampled during processing and 10 x 10 m pixels were generated from the original ~4.2 x11.4 m

pixels. The subscene in Figure 15B is a full resolution image of this resampled data as it was displayed on the image processing monitor. The number of pixels in this undecimated subscene is 262,000 (the monitor displays 512 x 512 pixels); therefore the area displayed is only ~5 x 5 km^2. This area is outlined in Figure 15A. Although this contrast stretching was accomplished on a relatively small area, full-resolution stretching was found to be more informative than working with decimated images that covered a larger ground area.

The oversaturated (bright) cliffs outlined on Figure 15A had reflectances that ranged from 100 to 210 on a scale of 0 (pure black) to 255 (pure white). The subscene (Figure 15B) was interactively manipulated and the example shown is one where reflectance values below 100 were saturated to pure black (0) and those from 100 to 210 were stretched over the full range of 0 to 255. Contrast stretching of the brightest digital values (at the expense of the rest of the scene) does reveal subtle topographic and structural information along south-facing cliffs. This new information could not be discerned on the original, balanced imagery.

11.0 REFERENCES

Brown, C. M. and G. P. Robinson (compilers), 1982, Kutubu, Papua New Guinea 1:250,000 Geological Series - Explanatory Notes, Sheet SB/54-12 International Index: Department of Minerals and Energy, Australia and Geological Survey of Papua New Guinea, 43 p., 1 map sheet.

Davies, H. L., (compiler), 1983, Wabag, Papua New Guinea 1:250,000 Geological Series - Explanatory Notes, Sheet SB/54-8 International Index: Department of Minerals and Energy, Australia and Geological Survey of Papua New Guinea, 84 p., 1 map sheet.

Davies, H. L. and M. Norvick (compilers), 1974, Blucher Range, Papua New Guinea 1:250,000 Geological Series - Explanatory Notes, Sheet SB/54-8 International Index: Department of Minerals and Energy, Australia and Geological Survey of Papua New Guinea, 29 p., 1 map sheet (OK Tedi is revised name of sheet).

Dahlstrom, C. D. A., 1969, Balanced cross sections: Canadian Journal of Earth Sciences, v. 4, no. 6, p. 743-757.

Dow, D. B., 1977, A geological synthesis of Papua New Guinea: Bureau of Mineral Resources, Australia, Bulletin 201, 41 p.

Francis, G., J. M. James, D. S. Gillieson, and N. R. Montgomery, 1980, Underground geomorphology: in J. M. James and H. J. Dyson, eds., Caves and Karst of the Muller Range - Exploration in Papua New Guinea: A. T. Sutton & Co. (ISBN 086758 042 9), Australia, p. 111.

Hobson, D. M., 1986, A thin-skinned model for the Papuan thrust belt and some implications for hydrocarbon exploration: Australasian Petroleum Exploration Association Ltd. Conference, Adelaide, April 7-9, 1986, v. 26, part 1, p. 214-224.

Jenkins, D. A. L., 1974, Detachment tectonics in western Papua New Guinea: Geological Society of America Bulletin, v. 85, p. 533-548.

Jensen, H., L. C. Graham, L. J. Porcello, and E. N. Leith, 1977, Side-looking airborne radar: Scientific American, v. 237, no. 4, p. 84-95.

Sabins, F. F., 1983, Geologic interpretation of space shuttle radar images of Indonesia: American Association of Petroleum Geologists Bulletin, v. 67, no. 11, p. 2076-2099.

Sabins, F. F., 1986, Remote sensing - principles and interpretation, second edition: W. H. Freeman & Co., New York, 449 p.

Smith, J. G., 1965, Orogenesis in Western Papua and New Guinea: Tectonophysics, v. 2, no. 1, p. 1-27.

Thornbury, W. D., 1969, Principles of Geomorphology, second edition: Wiley, New York, p. 303-344.

Wing, R. S. and H. C. MacDonald, 1973, Radar geology - petroleum exploration technique, Eastern Panama and Northwestern Colombia: American Association of Petroleum Geologists Bulletin, v. 57, no. 5, p. 825-840.

13.0 ACKNOWLEDGEMENTS

We are grateful to Chevron Overseas Petroleum Inc., Niugini Gulf Oil Pty. Ltd. (a Chevron-owned company and operator), and the Joint Venture Partners of the PPL-17 and PPl-18, Papua New Guinea exploration licenses:

Merlin Petroleum Company
Pioneer Concrete (Bougainville) Pty. Ltd.[1]
BP Petroleum Development Australia Pty. Ltd.[2]
Ampol Exploration Pty. Ltd.
Australasian Petroleum Company Pty. Ltd.
(composed of BHP Petroleum Pty. Ltd., Oil Search Ltd., and 1 and 2 above)

for granting permission to publish this paper. We also express our appreciation to the Bureau of Mineral Resources, Australia and the Geological Survey of Papua New Guinea for approval to reproduce their excellent geological maps. The staff at Niugini Gulf Oil Pty. Ltd. (in particular, E. H. Gurney and H. E. James) were instrumental in providing geological information to us and arranging for a field visit to the southern fold and thrust belt of Papua New Guinea. We acknowledge proprietary data made available to the operator.

The Chevron Overseas Petroleum Inc. graphics and word processing personnel were extremely helpful in preparing this paper.

Mars Associates, Inc. constructed an excellent radar mosaic and completed the initial interpretation of the SAR data. R. H. Gelnett of Mars Associates, Inc. was especially helpful in organizing the survey and ensuring we understood the interpretative aspects of SAR imagery. Intera Technologies Ltd. acquired the outstanding imagery using an X-band, synthetic aperture STAR-1 digital radar system. Rob Inkster of Intera has assisted in improving our understanding of the technical aspects of SAR acquisition.

F. F. Sabins, W. S. Kowalik and T. F. Battey of the Remote Sensing Lab at Chevron Oil Field Research Company accomplished the digital manipulation of the SAR and Landsat data. F. F. Sabins also provided timely geological and technical advice, and reviewed our paper.

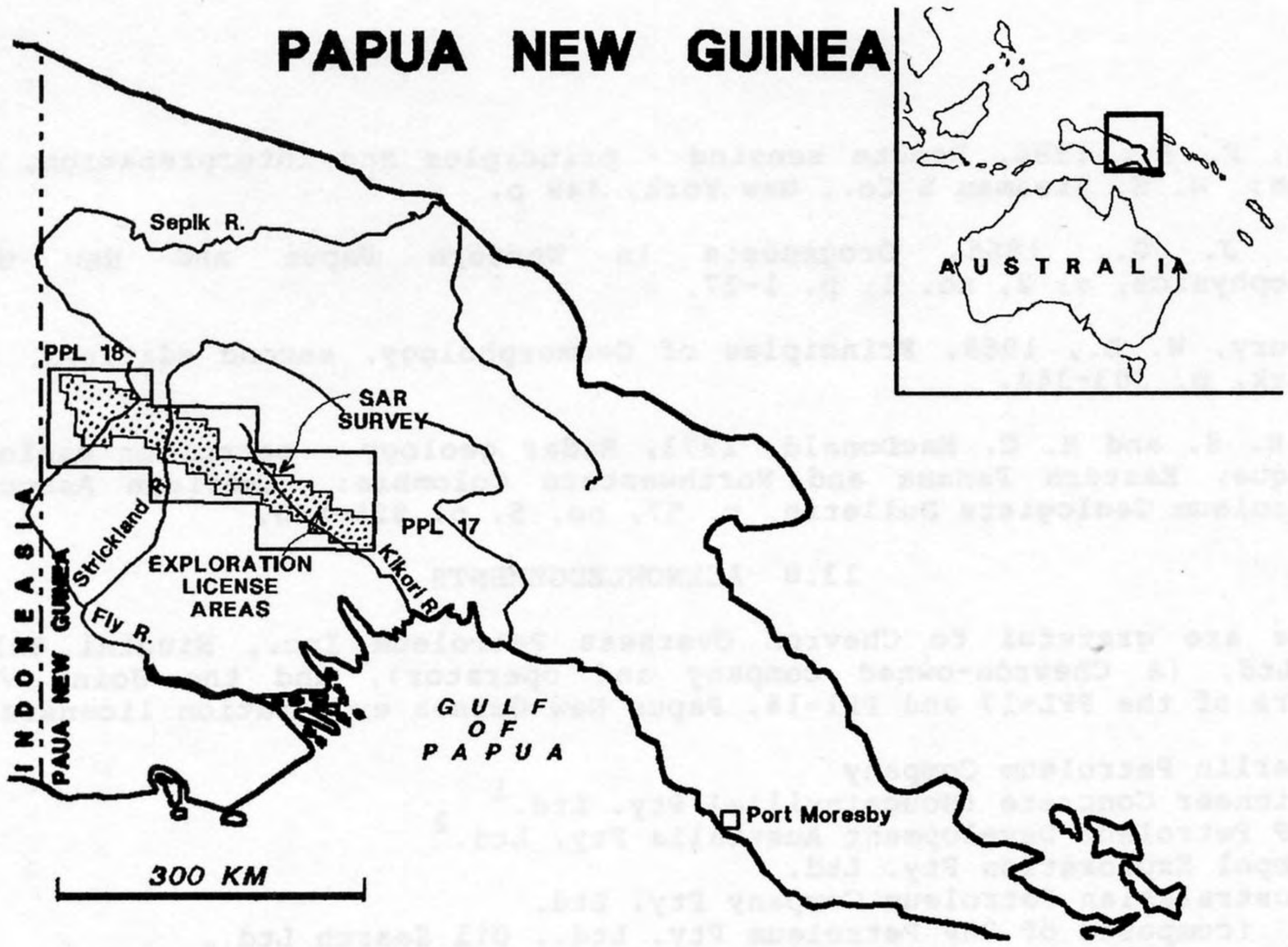

Figure 1. Location map showing Papua New Guinea, area of exploration licenses PPL-17 and -18, and area surveyed by SAR (~26,000km^2).

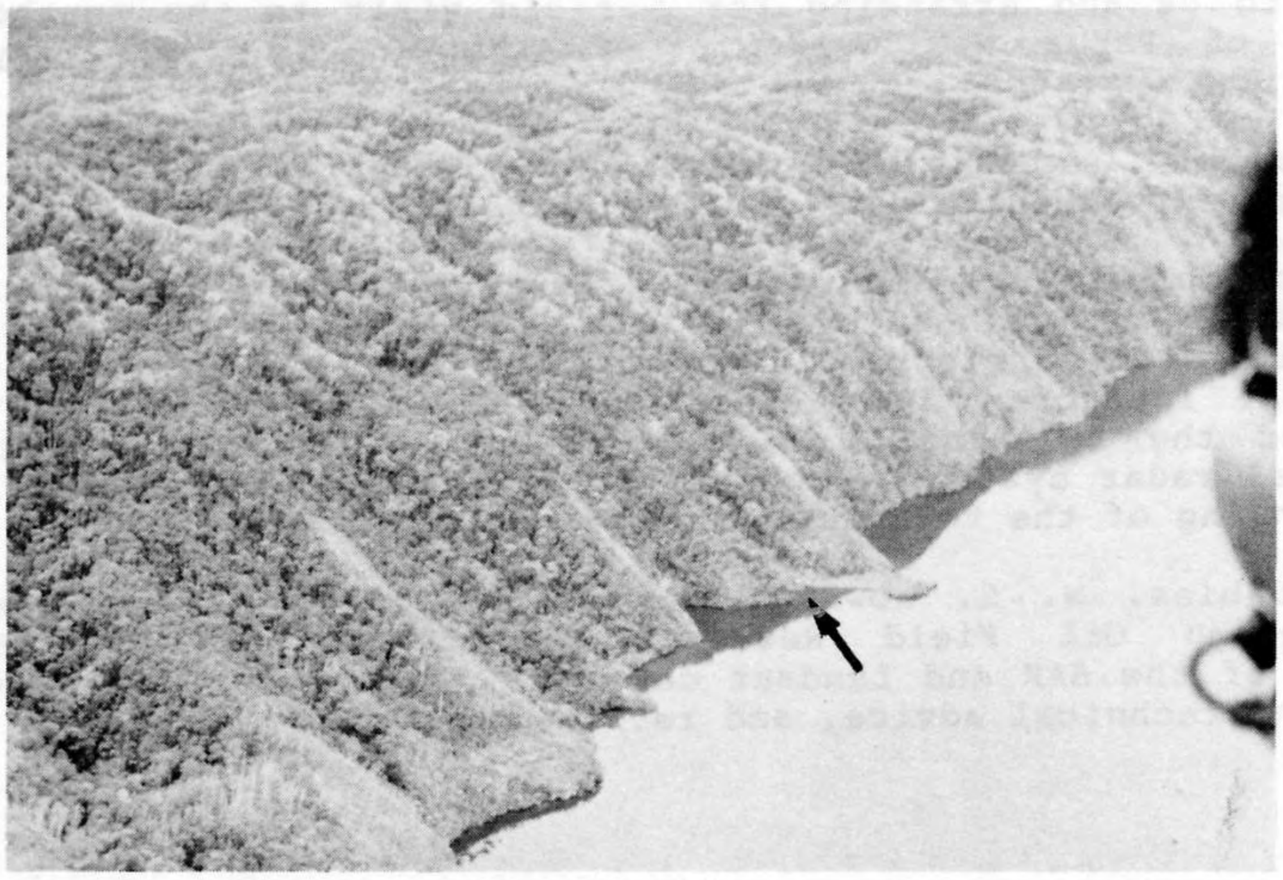

Figure 2. Darai Limestone dips steeply on the flank of Kutubu anticline. Small huts can be seen along the shoreline for scale. Topographic relief from lake to crest of anticline is 500 m. Rugged karst topography has developed on the limestone, making seismic technology impractical.

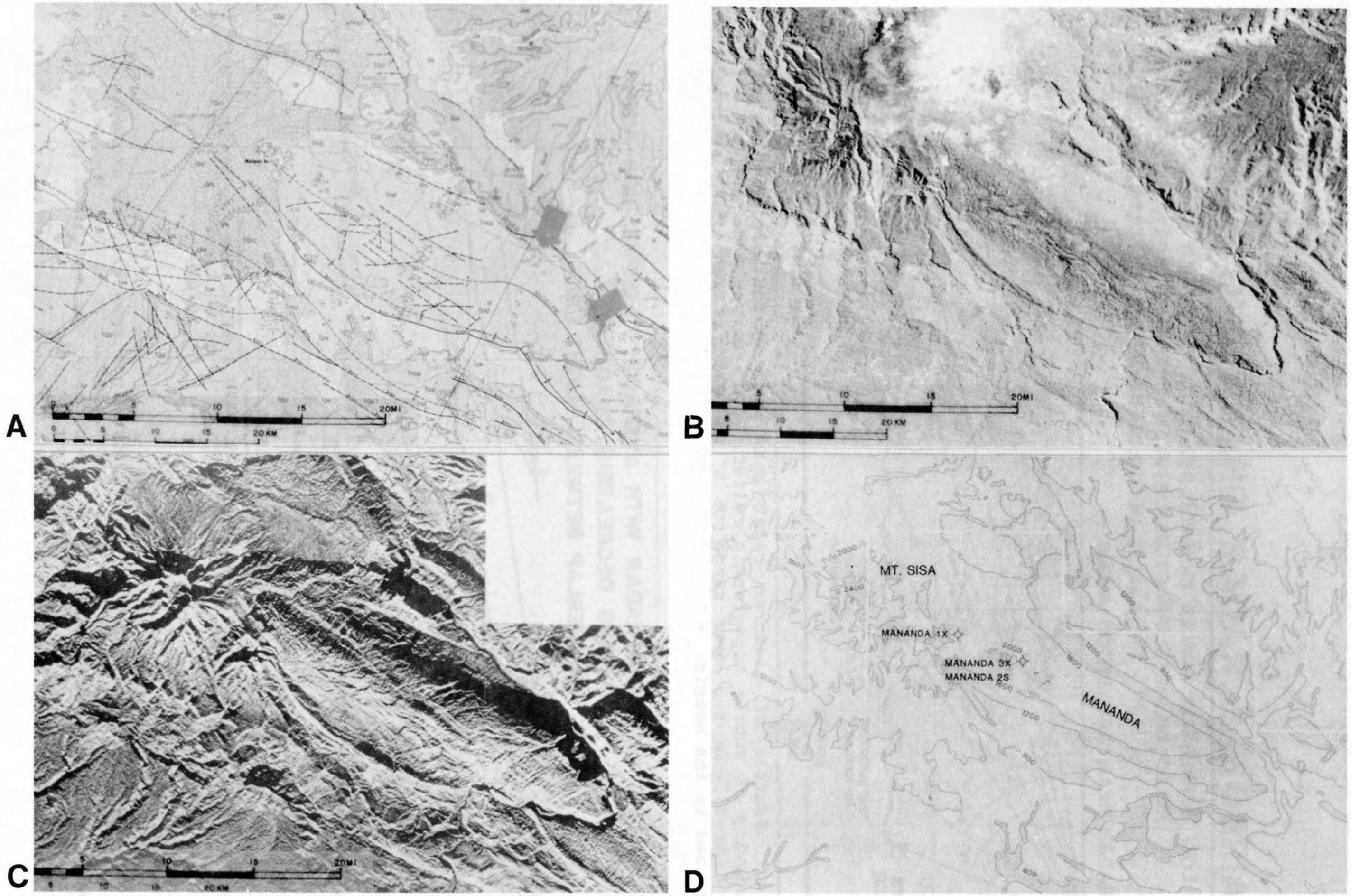

Figure 3. Example of data set available for the exploration effort, set at the same scale: (A) published geologic map, (B) Landsat MSS imagery, (C) SAR imagery, and (D) simplified topographic map (400 m contour interval). Arrows on map point to topographic scarps that are best evaluated with Landsat and SAR. SAR reveals widespread surface instability along illuminated (south) flank of Mananda anticline. Figures 8, 11, 12, and 15 are enlargements of portions of this region.

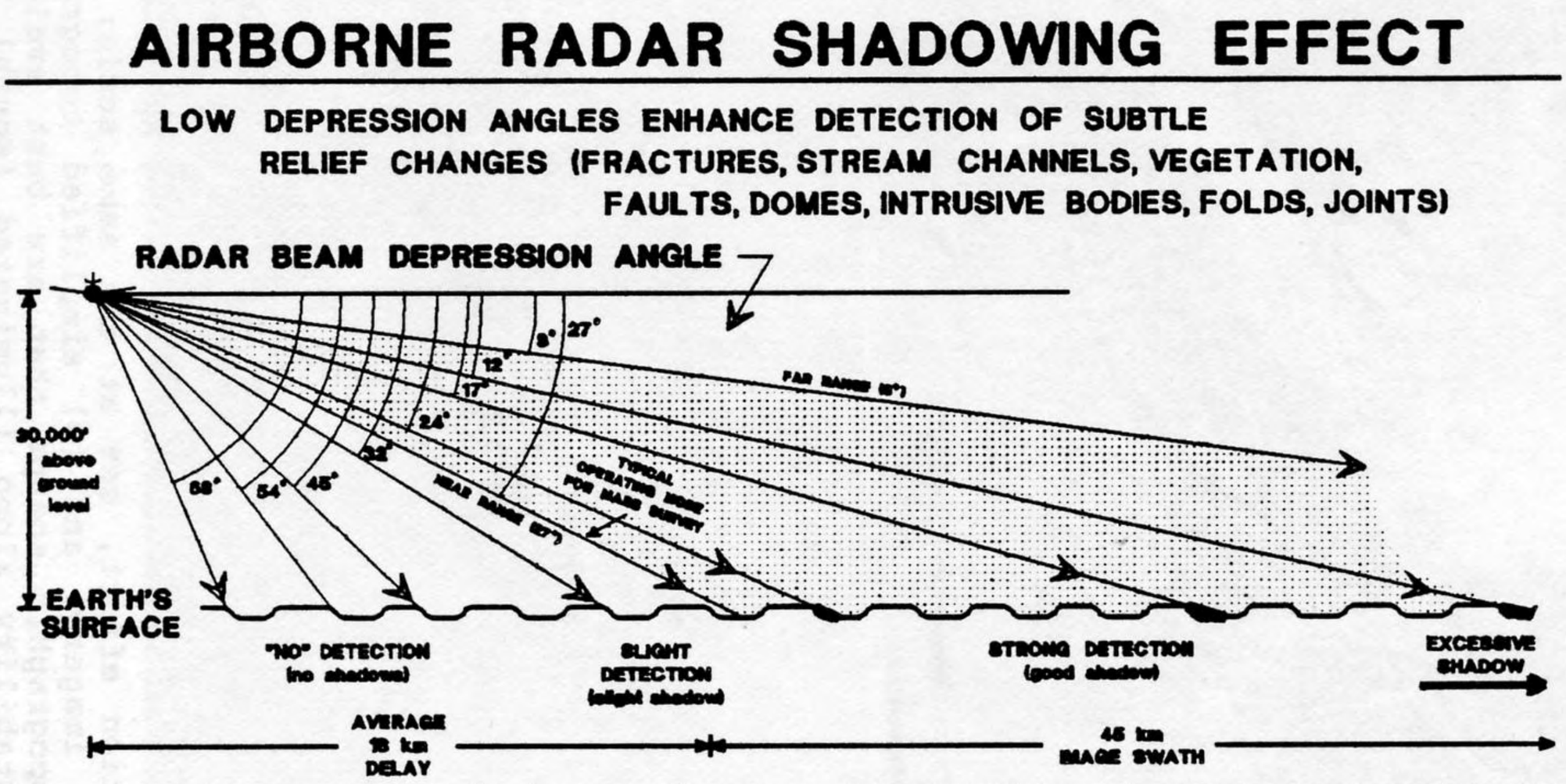

Figure 4. Profile of airborne radar beam with various depression angles and shadowing of subtle topographic relief. This survey's depression angles ranged from 27° in the near range to 8° in the far range; an average of 17° was used in the mosaic. -

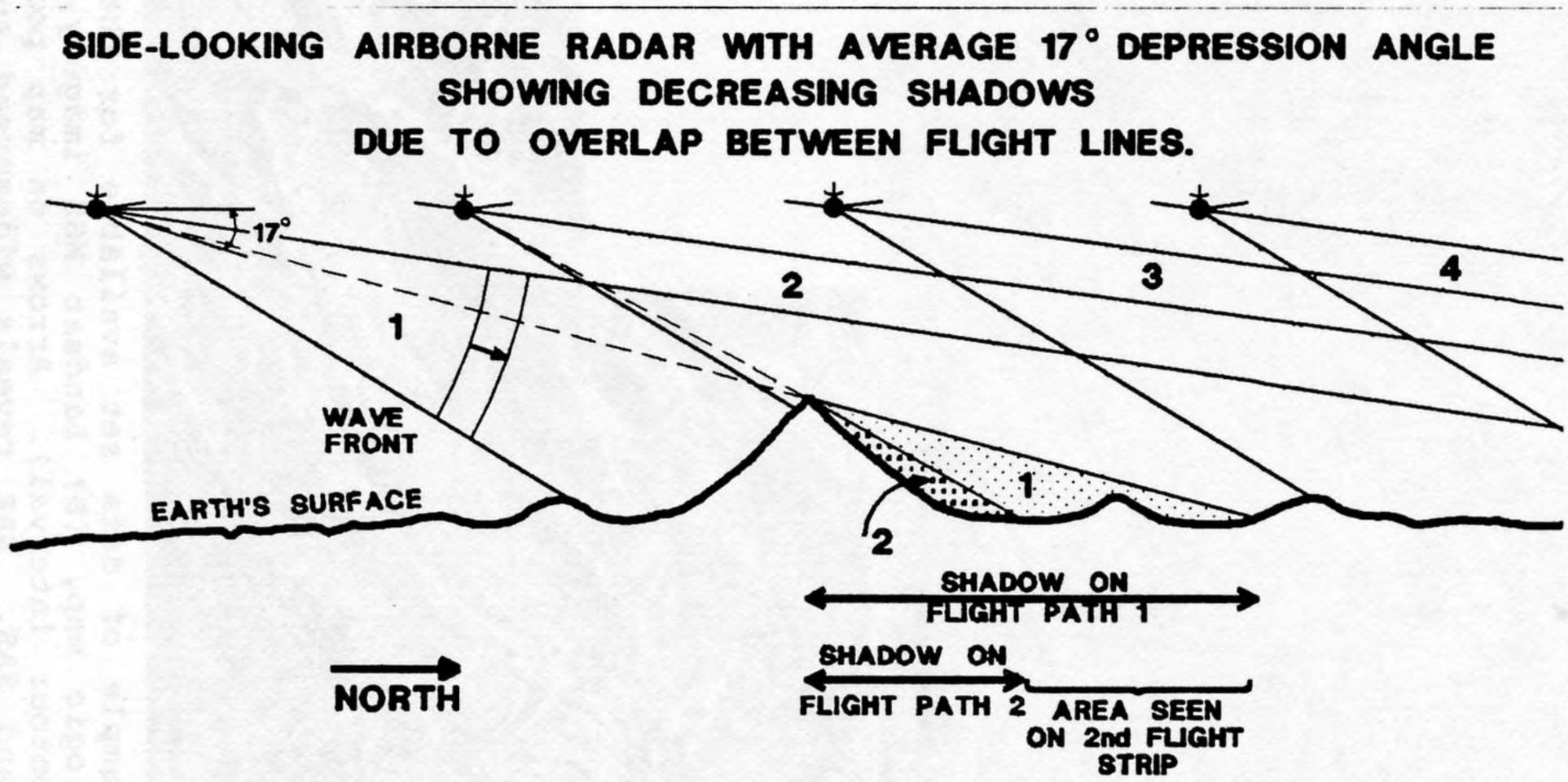

Figure 5. Profile of overlapping SAR flight lines resulting in stereoscopic flight strips and reduction in the area hidden by radar shadow. The detrimental effect of shadowing due to topography was minimized by mapping in the near-range portion of the stereo flight strips.

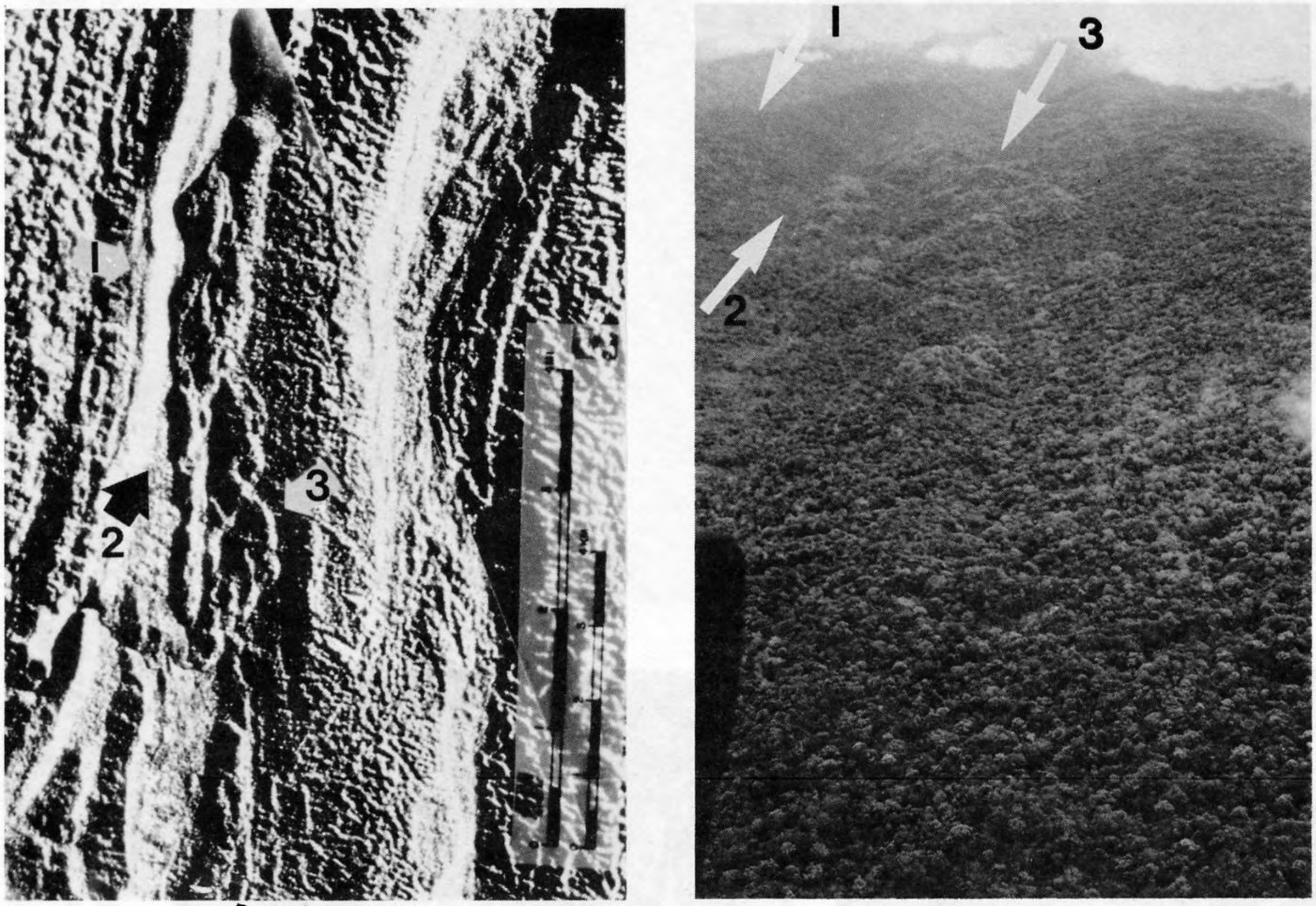

Figure 6. Comparison of radar image with color photo of a (1) thrust fault carrying Darai Limestone over shales, (2) stratigraphic contact between shales and resistant limestone, and (3) outcrop pattern of Darai strata folded into an anticline. Pitted and irregular radar signature of deeply weathered limestone contrasts with smooth, medium-gray signature of shales.

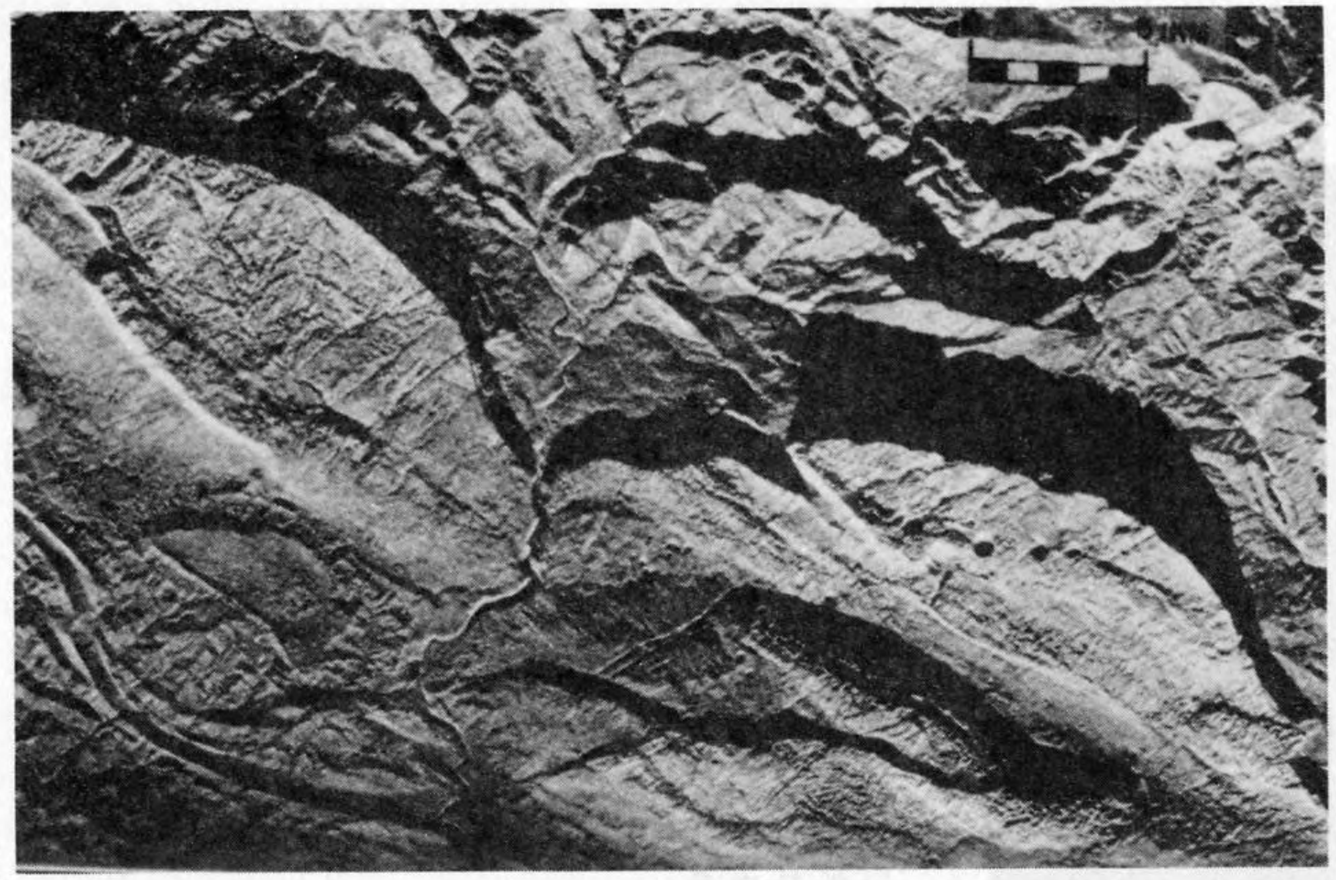

B

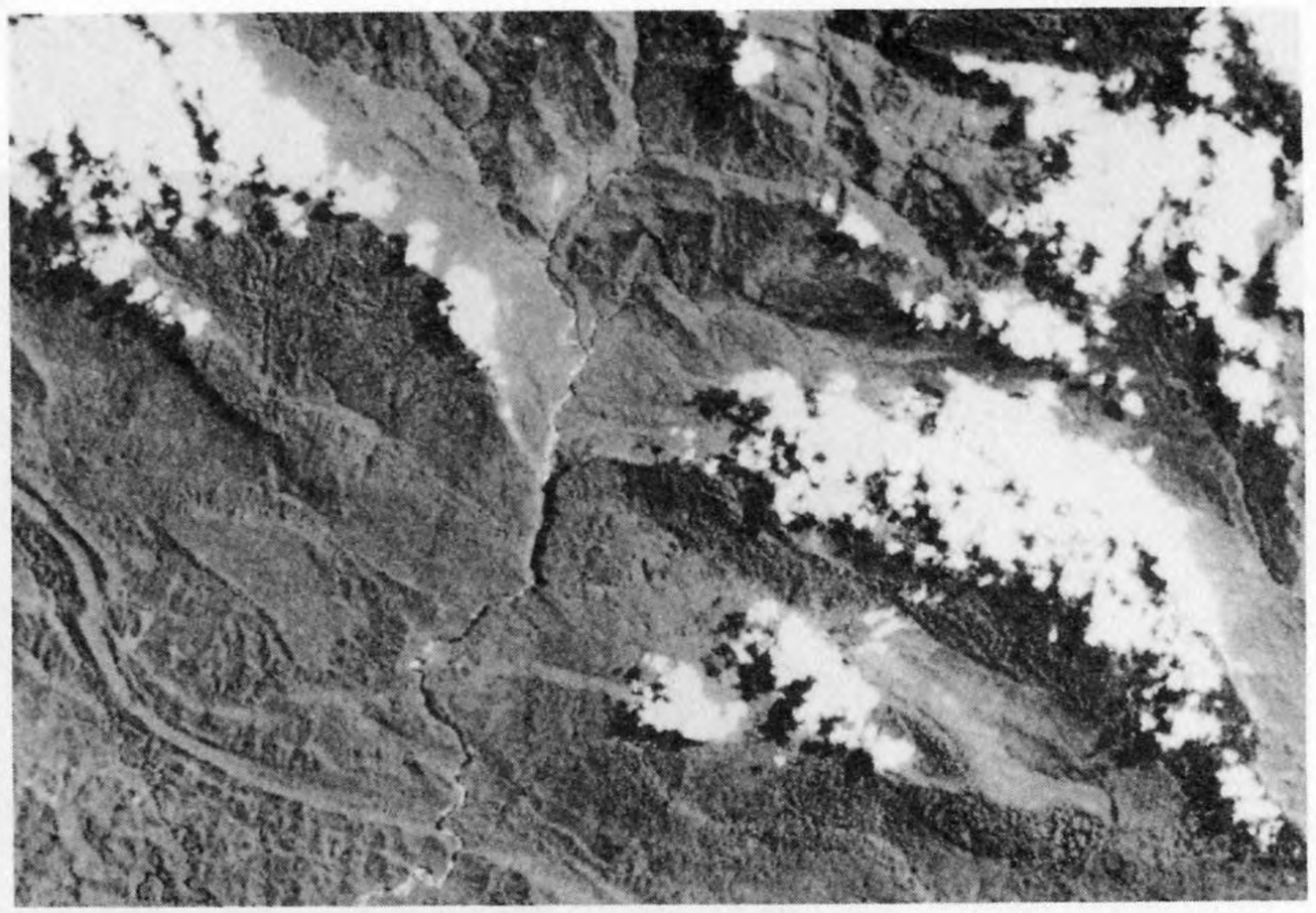

C

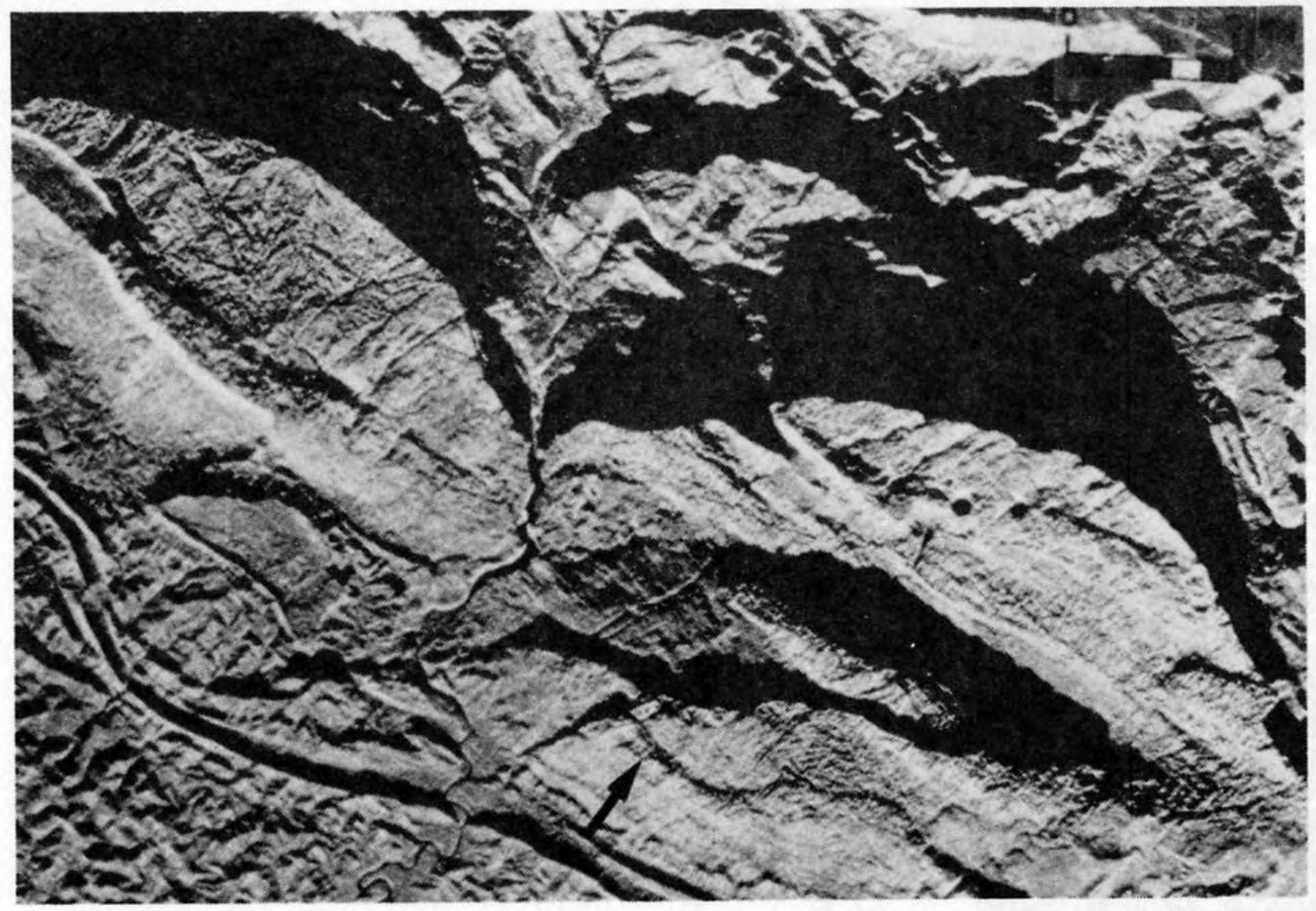

A

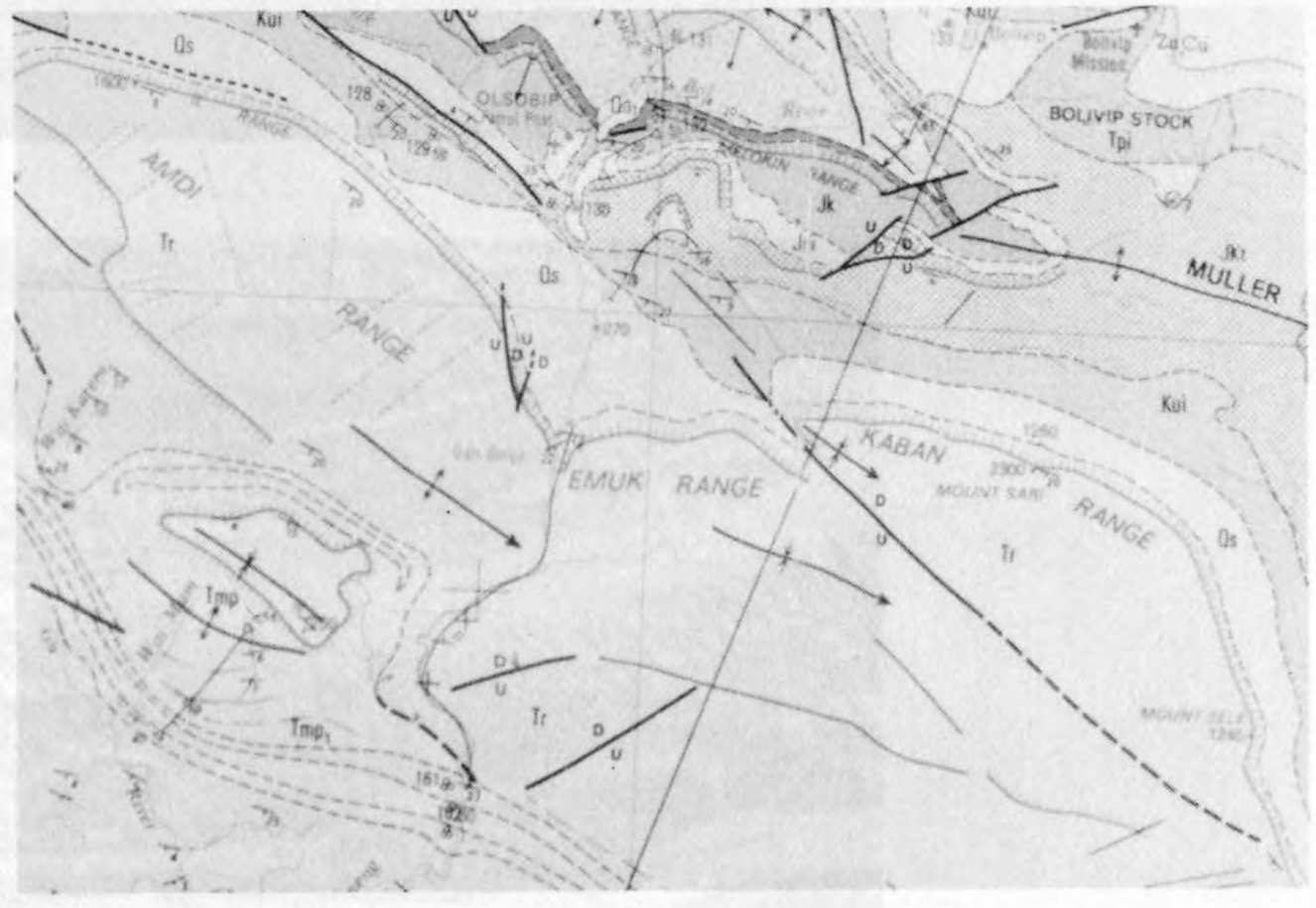

D

Figure 7. SAR stereopair (A and B) compared for geological information with same-scale plots of the Landsat MSS image (C) and published geologic map (D). The near-range portion of flight strip (B) has more terrain illuminated than the mid-range image (A) due to the steeper depression angle of the radar beam. Two unmapped anticlines are clearly seen on SAR (arrow on A). The SAR imagery has the most structural and karst information.

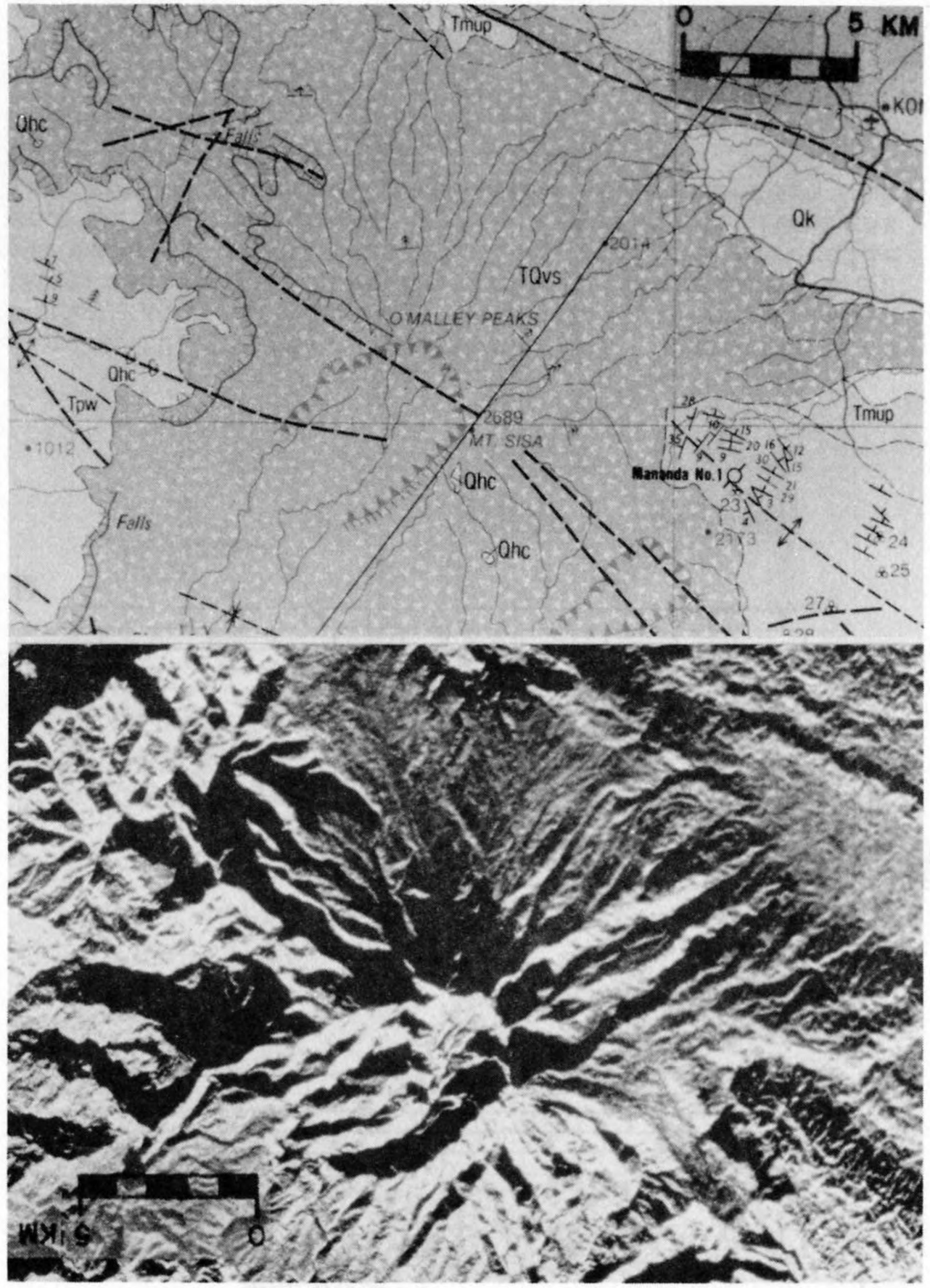

Figure 8. Suspected faults mapped on the geologic sheet as trending NW-SE through craters can be expanded upon with SAR. SAR shows valleys that trend NE-SW as deeply eroded into flanks of Mt. Sisa, suggesting a major zone of structural weakness.

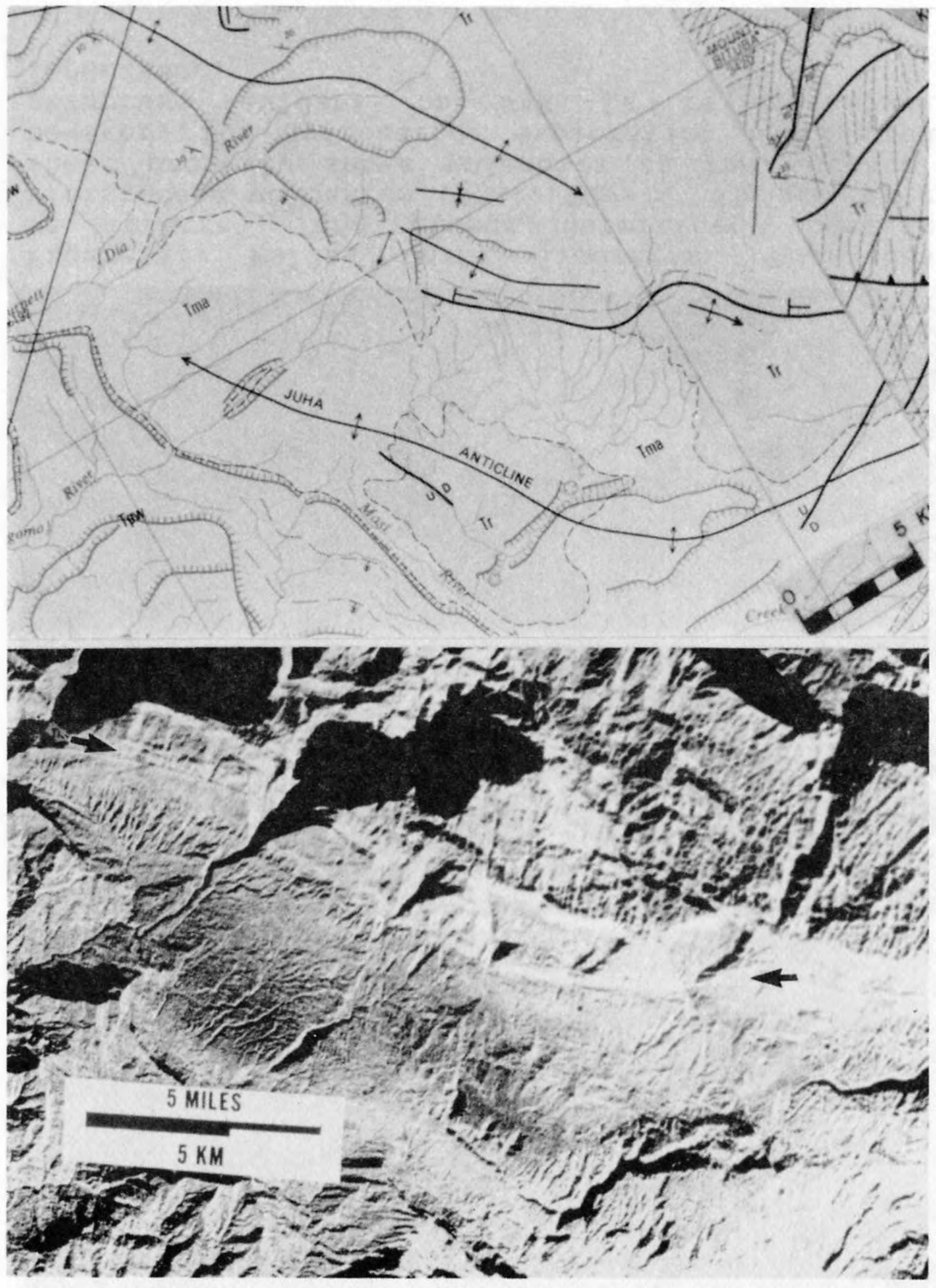

Figure 9. A band of resistant, upturned Darai Limestone (Tr) is highlighted with 2 arrows on the SAR image (NE is toward the upper margin of the same-scale image and map). A thrust fault is mapped only along the SE base of this strata. See text for discussion (Section 6.0).

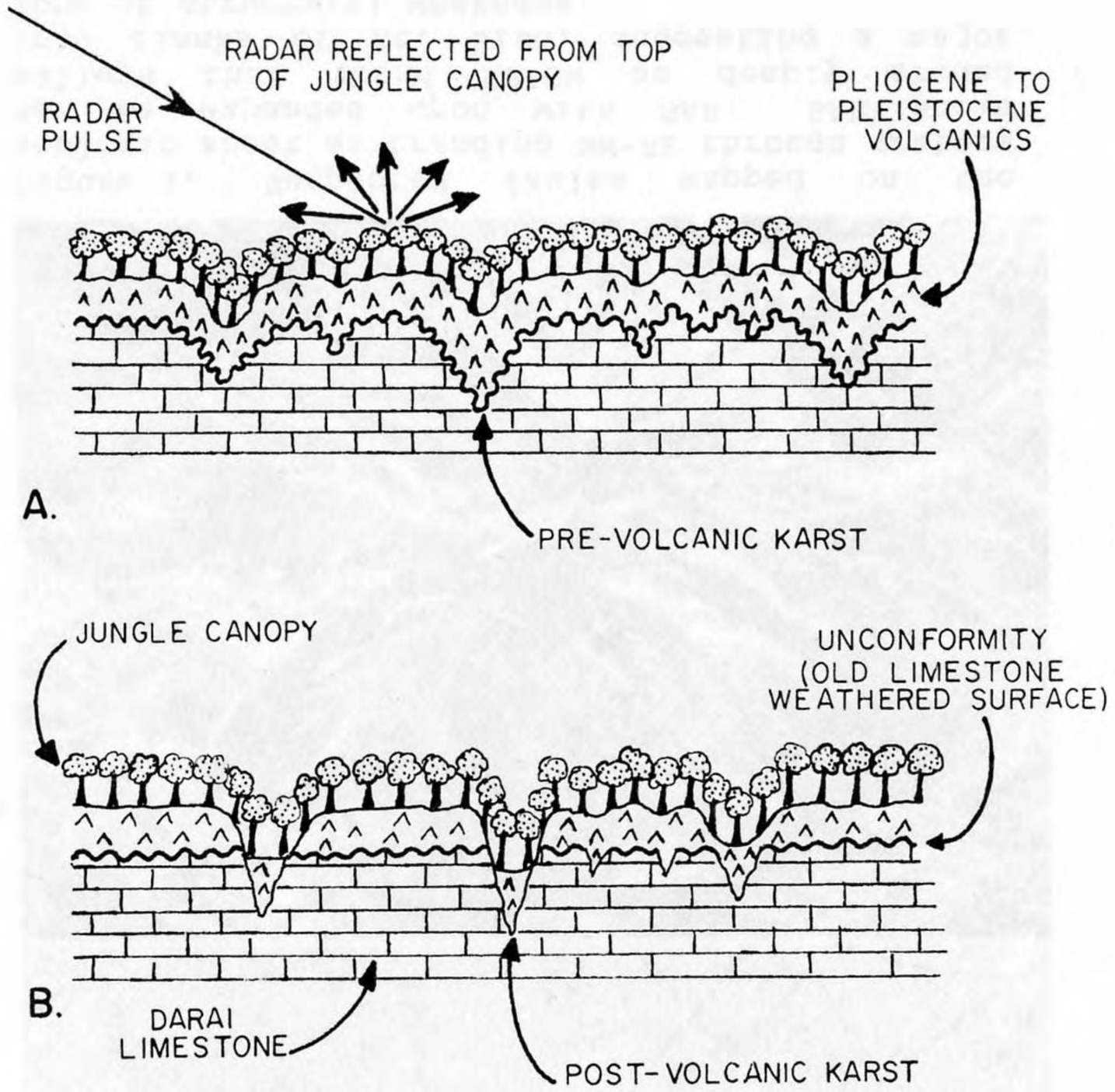

Figure 10. Darai Limestone is inferred as being buried beneath volcanic debris when the volcanics have a radar signature that is subtler than, but similar to, the irregular and pitted image of karst. Karst development in the limestone may have been before or coincident (A), or after (B) volcanic deposition.

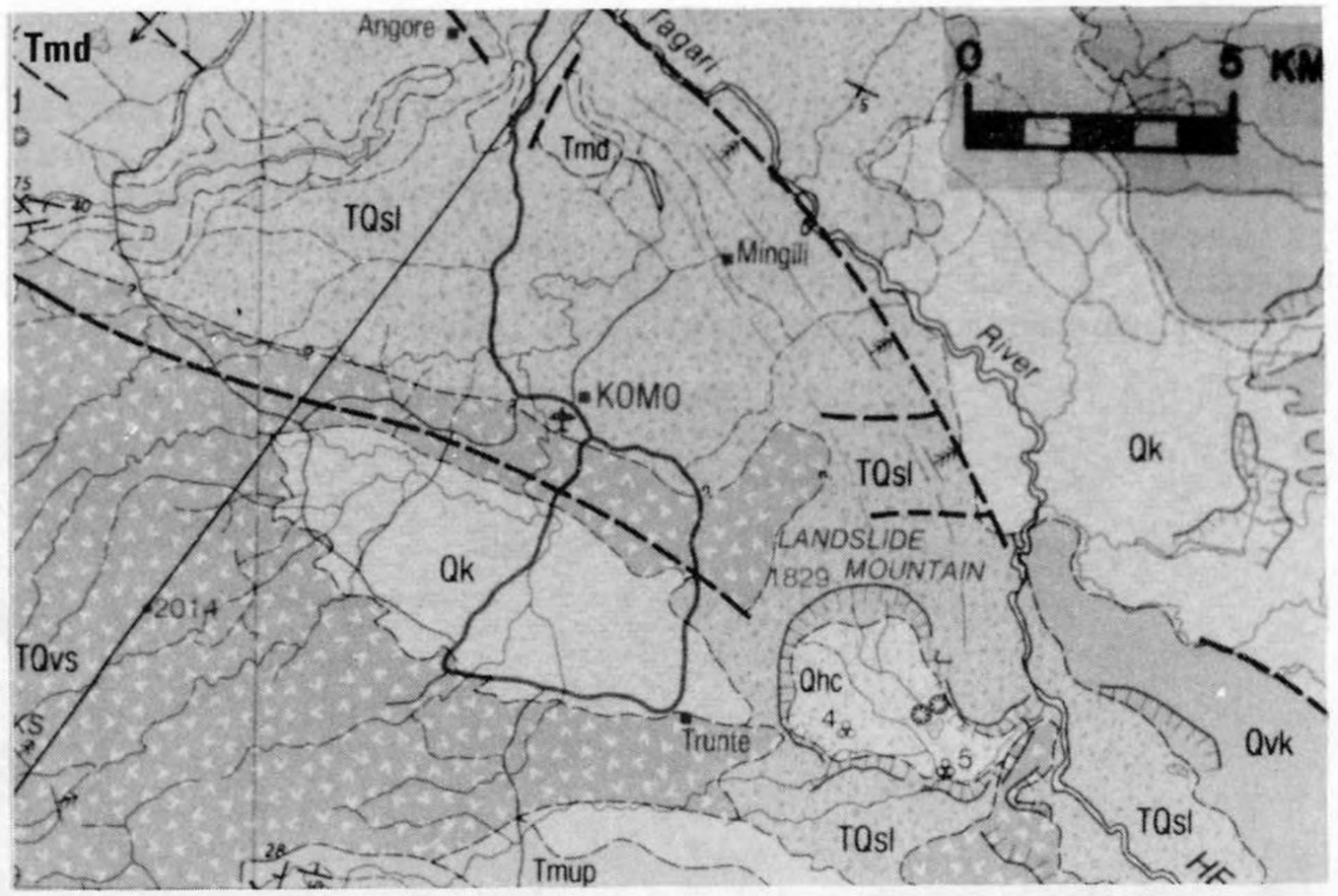

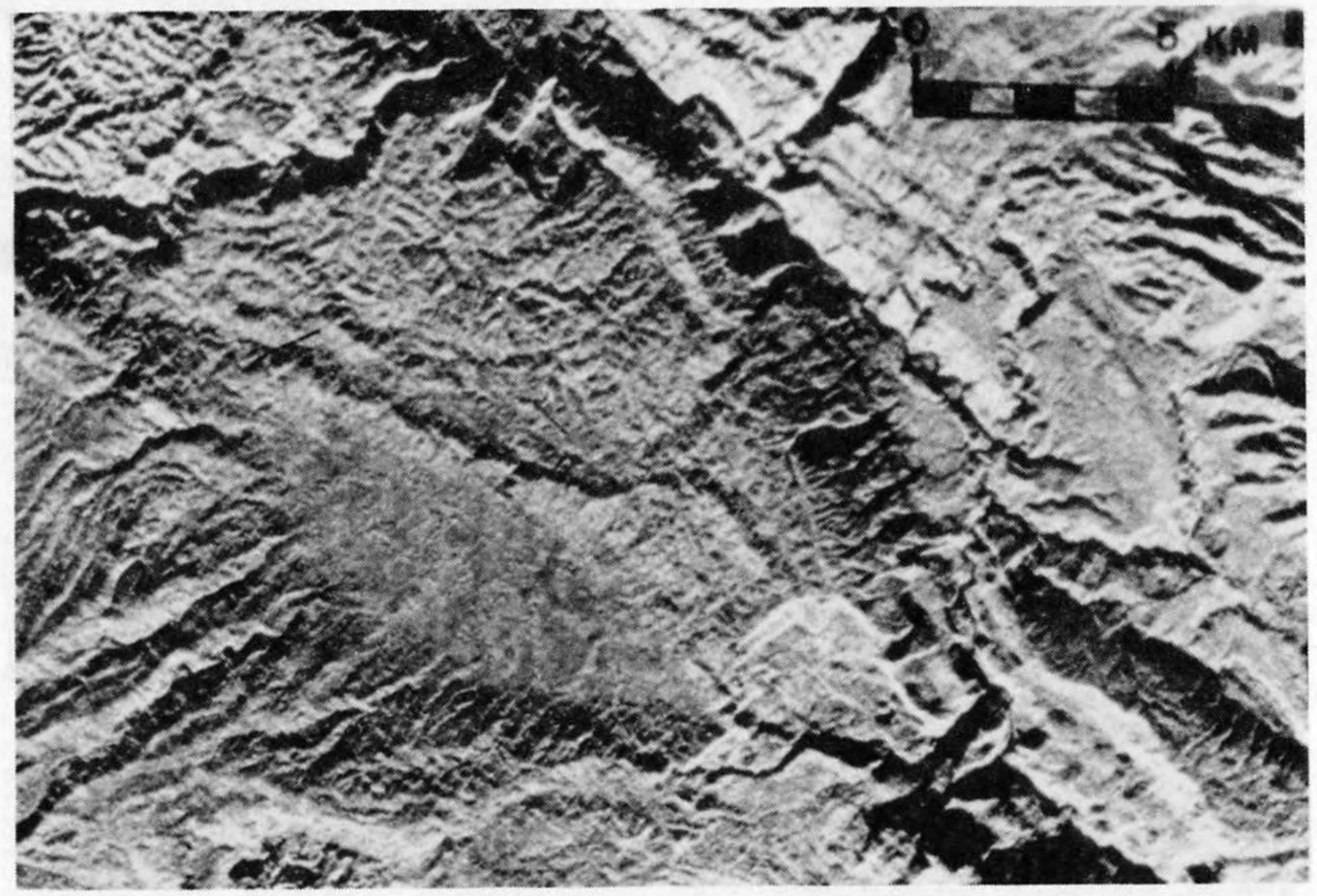

Figure 11. Folded Darai limestone (Tmd) can be inferred, and plunge determined, beneath Pleistocene volcanics (TQsl, TQvs). The geologic sheet properly shows volcanics at the surface; however, for hydrocarbon exploration the buried structure evident on SAR is of paramount importance.

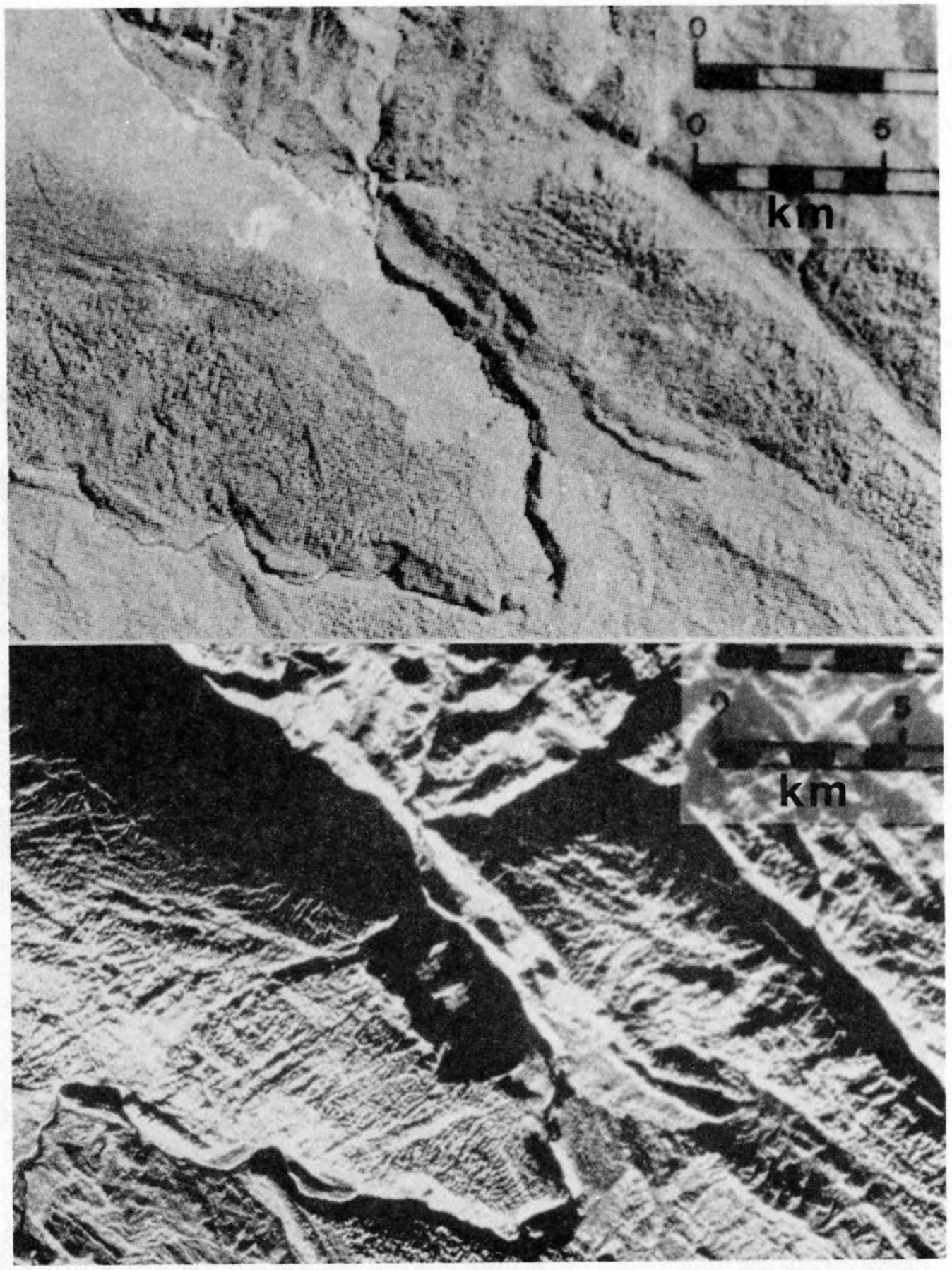

Figure 12. Recent rockslides along the NE nose of Manada anticline are best seen on Landsat as white scars. Major WSW-ENE topographic breaks across nose of anticline obvious on radar but very subtle on Landsat. See text for discussion (Section 8.0).

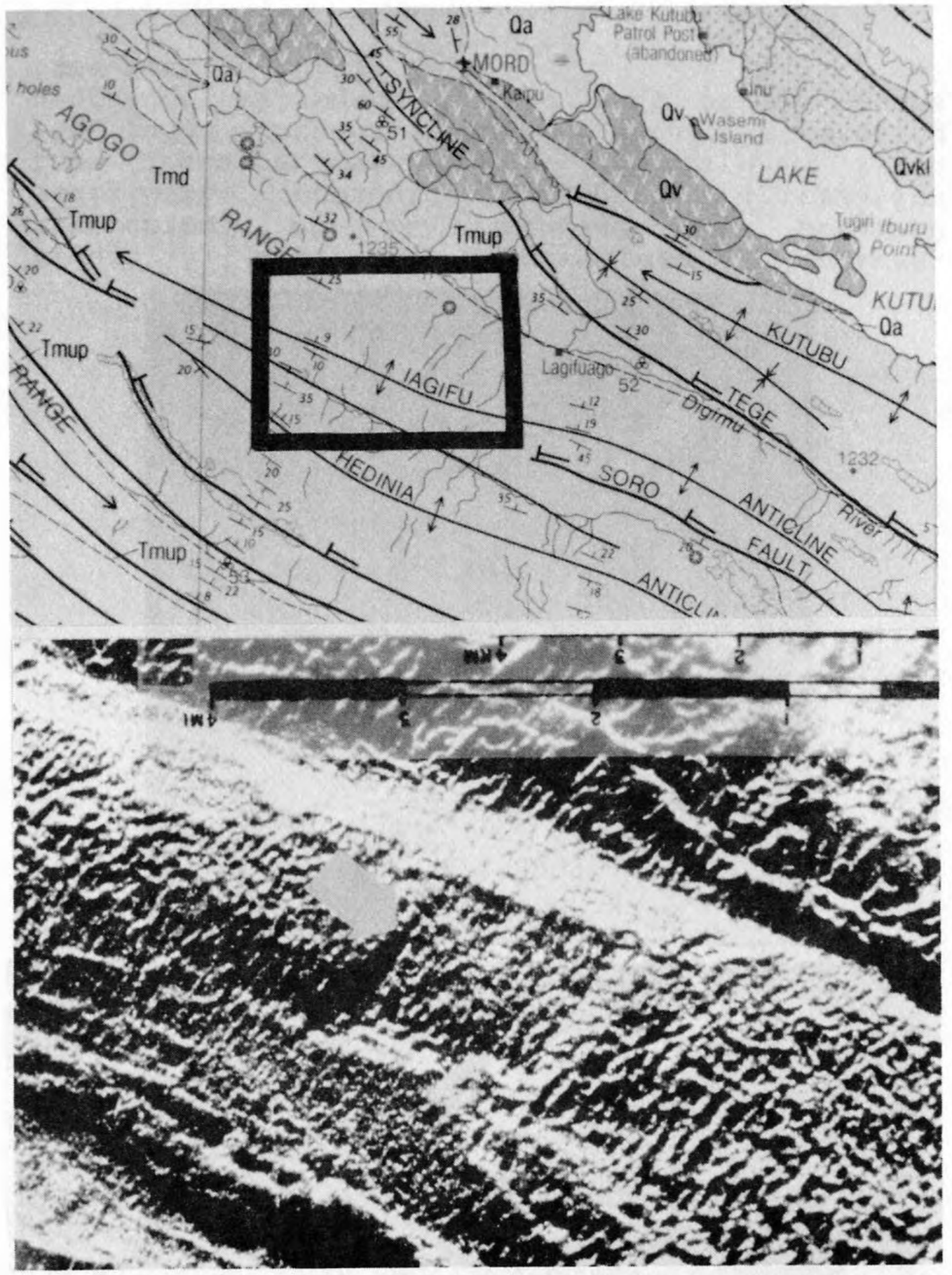

Figure 13. Large, downdropped block of limestone caprock seen along crest of an anticline on radar, but unmapped on smaller-scale map. The importance of these depressions to exploration depends on the geological process(es) controlling their formation (see Section 8.0).

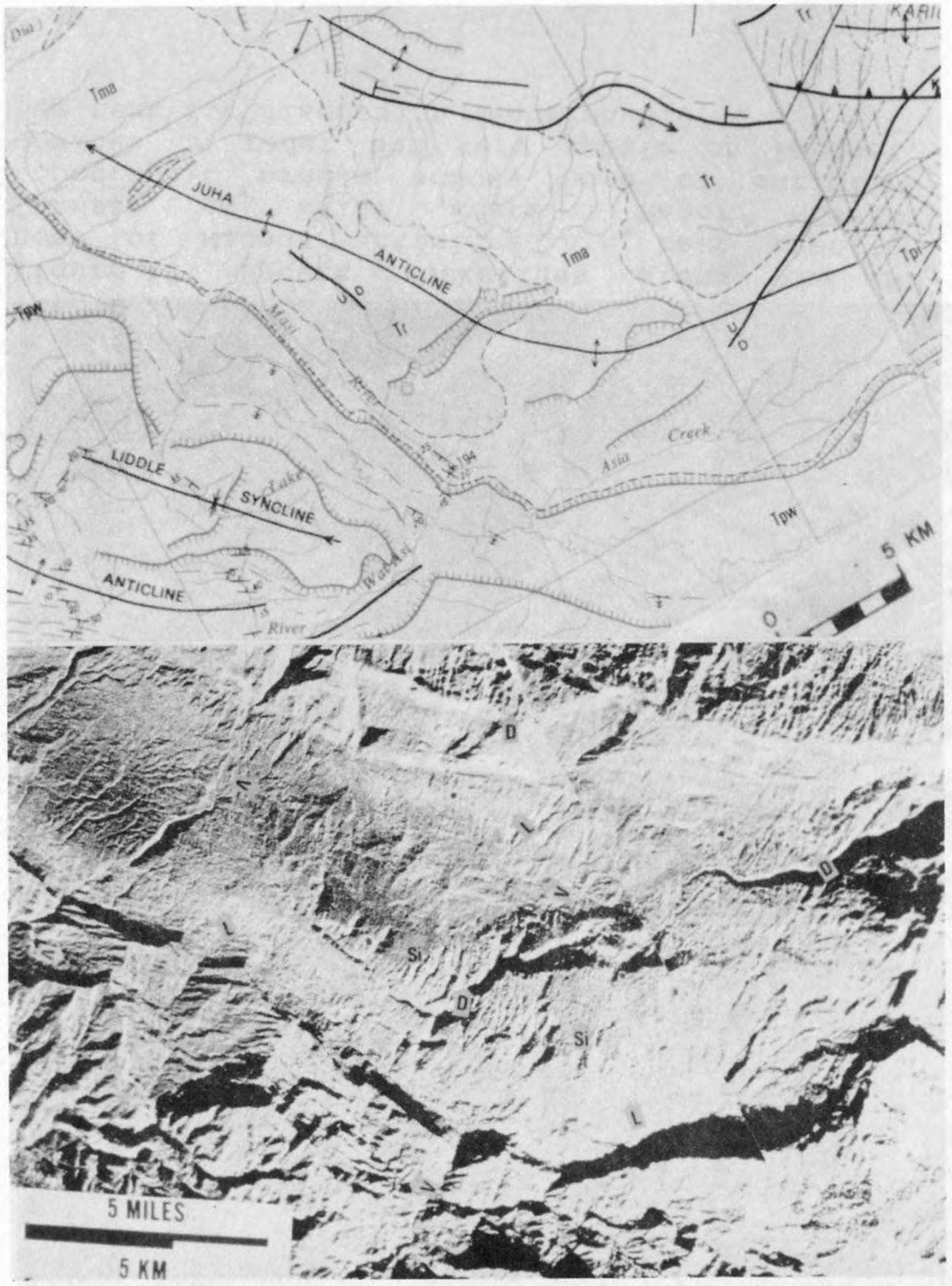

Figure 14. SAR image shows volcaniclastics (V), siltstones (Si), weak limestones (L), and tough Darai Limestone (D) at surface. NE is toward the upper margin of the same-scale image and map. Radar signatures for the same lithology vary across the E-W splice line (see Section 9.0).

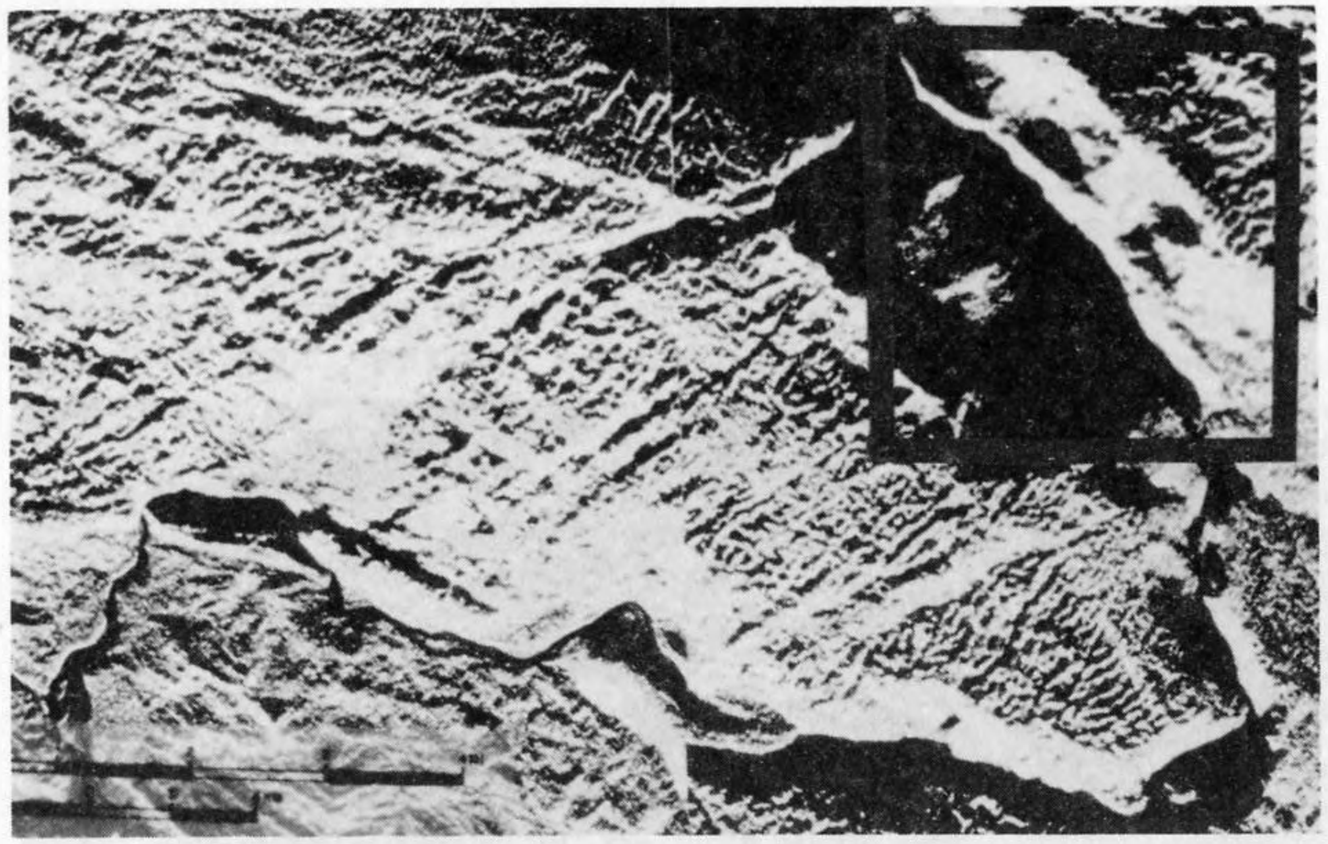

Figure 15. Digital reprocessing (contrast stretching) of SAR subscene (B) obtained additional geologic/topographic information from oversaturated (bright) cliffs that faced the radar antenna. This contrast stretching degraded (as expected) the rest of the scene (see Section 10.0).